ELSEVIER

Journal of Alloys and Compounds 388 (2005) 145–152

Journal of ALLOYS AND COMPOUNDS

www.elsevier.com/locate/jallcom

The effects on the structures and properties in the oxide-ion conductor $La_2Mo_2O_9$ by partial substituting Ba for La

Tianmin He[a,*], Yinglong Huang[a], Qiang He[a], Yuan Ji[a], Li Pei[a], Jiang Liu[a], Zhe Lu[b]

[a] *College of Physics, Jilin University, Changchun 130023, PR China*
[b] *Center for Condensed Matter Science and Technology, Harbin Institute of Technology, Harbin 150001, PR China*

Received 22 December 2003; received in revised form 14 July 2004; accepted 14 July 2004

Abstract

The oxide-ion conductors $(La_{1-x}Ba_x)_2Mo_2O_{9-\delta}$ (x = 0.02–0.10) were prepared by a solid-state reaction method. The formation process of the $La_2Mo_2O_9$ phase in the samples was investigated using a thermal dilatometer. The effects on the structures and properties in the oxide-ion conductor $La_2Mo_2O_9$ by partially substituting Ba for La were studied using X-ray diffraction, ac impedance spectroscopy and thermal dilatometry, respectively. The minimum doping content of Ba, which can suppress the structural phase transition in $La_2Mo_2O_9$, and the solubility of Ba in $(La_{1-x}Ba_x)_2Mo_2O_{9-\delta}$, was determined. The results show that the formation process of the $La_2Mo_2O_9$ phase presents an expansion process due to the introduction of oxygen vacancies. With the increase of the Ba doping contents, the lattice constant decreases at first and then increases. The lattice constant attains a peak at x = 0.08, and therefore, it is concluded that the solid solution limit of Ba in $(La_{1-x}Ba_x)_2Mo_2O_{9-\delta}$ is around x = 0.08. When x > 0.02, the structural phase transition in $La_2Mo_2O_9$ can be completely suppressed through the partial substitution of Ba for La as demonstrated by the observation of both electrical and thermal properties. For x = 0.08, the conductivity of the oxide-ion conductor $(La_{1-x}Ba_x)_2Mo_2O_{9-\delta}$ reaches a maximum of 0.046 and 0.075 S/cm at 800 and 850 °C, respectively.

Keywords: Oxide-ion conductors; $La_2Mo_2O_9$; Substitution; Structural phase transition; Ion conductivity

1. Introduction

Solid electrolytes are metastable phases between room temperature and the melting points, in which conducting carriers are ions. In a solid electrolyte, only special ions can migrate, and therefore various kinds of devices such as ionic sensors, solid oxide fuel cells (SOFCs), oxygen pumps and memory components can be fabricated through the use of the ion selectivity. In solid electrolytes, oxide-ion conductors have attracted much attention due to their technical and potential applications. At present, among oxygen ion conductors, there are four main, distinct structures [1–4]: cubic fluorite, perovskite, intergrowth perovskite/Bi_2O_2 layers and pyrochlore. Recently, Lacorre et al. [5] reported a new oxygen ion conductor $La_2Mo_2O_9$, which has a structure different from the above four structures. For this compound, the high temperature form of the $La_2Mo_2O_9$ is similar to that of β-$SnWO_4$ structure. That is, the high temperature form of β-$La_2Mo_2O_9$ has a cubic structure, cell parameter a = 7.2014(5) Å, space group $P2_13$ (no. 198), while the low temperature form has a much more complex structure [6–7]. Compared to other oxygen ion conductors as mentioned above, oxygen vacancies exist intrinsically for $La_2Mo_2O_9$, while the oxygen vacancies are introduced into the lattice as charge compensating defects by a partial substitution for other oxygen ion conductors. The $La_2Mo_2O_9$ can be considered as being formed by substitution of La^{3+} for Sn^{2+} in β-$SnWO_4$, and Mo^{6+} for W^{6+}. Divalent tin is a $5S^2$ lone-pair element, and the lone-pair occupies a volume similar to that of an O^{2-} anion, so that the $SnWO_4$ can be reformulated as $Sn_2W_2O_8E_2$. In $La_2Mo_2O_9$, the La^{3+} without the lone-pair replaced Sn^{2+} and its lone-pair, Mo^{6+} replaces W^{6+}, creates two extra vacancies due to charge compensation for the cation valence to increase. Then the formation of $La_2Mo_2O_9$ can be written $La_2Mo_2O_{8+1}\square$ and the extra

* Corresponding author. Tel.: +86-431-8185988; fax: +86-431-8921479.
E-mail address: hly@mail.jlu.edu.cn (T. He).

0925-8388/$ – see front matter © 2004 Elsevier B.V. All rights reserved.
doi:10.1016/j.jallcom.2004.07.010

vacancy allows for the oxygen ion conduction (here E indicates a lone-pair, and □ indicates a vacancy). This is the reason why $La_2Mo_2O_9$ is different from other oxygen ion conductors. The lone-pair substitution (LPS) concept has been proposed by Lacorre [8] to explain the above phenomenon. The LPS concept can be used to design and seek out novel oxygen ion conductors. $La_2Mo_2O_9$ exhibits a high ionic conductivity at 800 °C (around 0.06 S/cm). It can be completely used as electrolyte material for SOFC application by solely considering its conductivity. However, it undergoes a structural phase transition at around 580 °C [5], and the structural instabilities limit their further use in SOFCs. Therefore, it is important to suppress the structural phase transition in $La_2Mo_2O_9$, and to stabilize the high temperature form to low temperature. Various partial substitutions have been attempted on either the La site or Mo site or La and Mo sites as well as O site, in order to stabilize the high-temperature phase β-$La_2Mo_2O_9$ to room temperature [5,7,9–15]. The structural phase transition of $La_2Mo_2O_9$ can be suppressed through 10% Ba doping for $(La_{2-x}A_x)Mo_2O_9$ with A = Ba and $(La_{1-x}M_x)_2Mo_2O_{9-\delta}$ with M = Ba, as presented by Goutenoire et al. [7] and Subasri et al. [13]. However, these two groups only reported the lattice constant and electrical property of the 10% Ba doped-$La_2Mo_2O_9$, and the solid solution limit was not studied. We report here that an oxide-ion conductor $(La_{1-x}Ba_x)_2Mo_2O_{9-\delta}$ (x = 0.02–0.10) was prepared using a conventional solid-state reaction method. The effect of partially substituting Ba for La site on the structures and properties in the oxide-ion conductor $La_2Mo_2O_9$ were systematically investigated, and the solid solubility of Ba in $(La_{1-x}Ba_x)_2Mo_2O_{9-\delta}$ compounds was determined.

2. Experimental

2.1. Preparation of samples

La_2O_3 (99.99%), MoO_3 (99.5%) and $BaCO_3$ (99%) were used as starting materials, and La_2O_3 was pre-heated at 900 °C for 2 h before using, in order to remove the absorbed water and CO_2 in air. The powder of composition $(La_{1-x}Ba_x)_2Mo_2O_{9-\delta}$ (x = 0.02–0.10) was prepared by mixing the above materials in stoichiometric ratio. The weighted powders were ground in an agate mortar using ethanol as medium for 30 min, and then pressed into a mould to form pellet samples after drying. The pellet samples were calcinated at 500 °C for 12 h and pulverized and reground after cooling. Finally, the well-reground powders were pressed uni-axially into a cylinder sample of 6 mm in diameter and 2–3 and 5–6 mm in thickness at 200 MPa. Then the samples were sintered at 950 °C for 10 h in air, and the sintered samples were obtained after cooling.

2.2. Characterization of samples

The mixed powders of La_2O_3, MoO_3 and $BaCO_3$ were pressed uni-axially into a cylinder sample of Φ6 × 5–6 mm at 200 MPa. The sintering shrinkage curve was recorded using a horizontal pushrod dilatometer (Netzsch, DIL 402C). The thermal expansion curve was also measured for the sintered cylinder sample. The dilatometer was calibrated using the Netzsch Al_2O_3 standard. A small pressure of 5×10^{-3} N was applied to the samples by the pushrod of the dilatometer. For the above measurements, a heating rate of 5 °C/min was applied, and air was used as a purge gas with a flowing rate of 60 ml/min, with temperatures ranging from 30 to 1100 °C and 30 to 950 °C, respectively. The phase analysis for the sintered samples was determined using an X-ray diffractometer (Rigaku, D/Max-rA) with Cu Kα (λ = 1.5418 Å), a scanning range of 20–80 °. NaCl powder (99.9% pure) was used as the internal standard for the peak position determination. The lattice constants of the substituted compounds were calculated using a software package (Oxford Cryosystems). The real density of the sintered samples was measured using the standard Archimedes' method. The relative density is the ratio to real density and theoretical density. Silver paste (DAD-87) was used as an electrode to be painted on the two faces of the sintered sample, and silver wire as lead. Impedance spectra were performed using an impedance/gain-phase analyzer (Solartron SI 1260) for the sintered sample. The measuring frequency range was from 0.1 Hz to 3.2 MHz. The ac amplitude of 150 mV was applied, and the temperatures ranged from 300 to 850 °C in air. A Z-view 2.0 software was used to analyze the impedance data and to calculate the conductivity of the sintered samples.

3. Results and discussion

3.1. Sintering shrinkage curves of samples

Fig. 1 shows the typical sintering shrinkage curves for the compacted sample of mixed powders in air. Compared to the sintering shrinkage curve of common oxide-ion conductors, the sample showed a sharp expansion in the range of 430–520 °C. This was because oxygen vacancy was introduced during the La_2O_3, MoO_3 and $BaCO_3$ reaction to form $La_2Mo_2O_9$ phase, and the unit cell volume was increased, so that the expansion process was displayed [16]. The forming process of $La_2Mo_2O_9$ phase has been confirmed at this stage in our previous work [17], in which we used X-ray diffraction to detect the forming process of $La_2Mo_2O_9$ phase at different temperatures (see inset in Fig. 1). On the other hand, the expansion process shown in the curves likely came from the contribution of CO_2 due to a departure of CO_2 occurring during the reaction. The shrinkage curves were under expansion over a range of 520–720 °C. This indicated that the $La_2Mo_2O_9$ phase was being crystallized over the temperature range. The sintering shrinkage curves of the samples began to descend over the temperature range of 720–980 °C, showing that this temperature range was a sintering densification stage for $(La_{1-x}Ba_x)_2Mo_2O_{9-\delta}$ samples. Beyond 980 °C, the shrinkage curves sharply dropped, indicating that

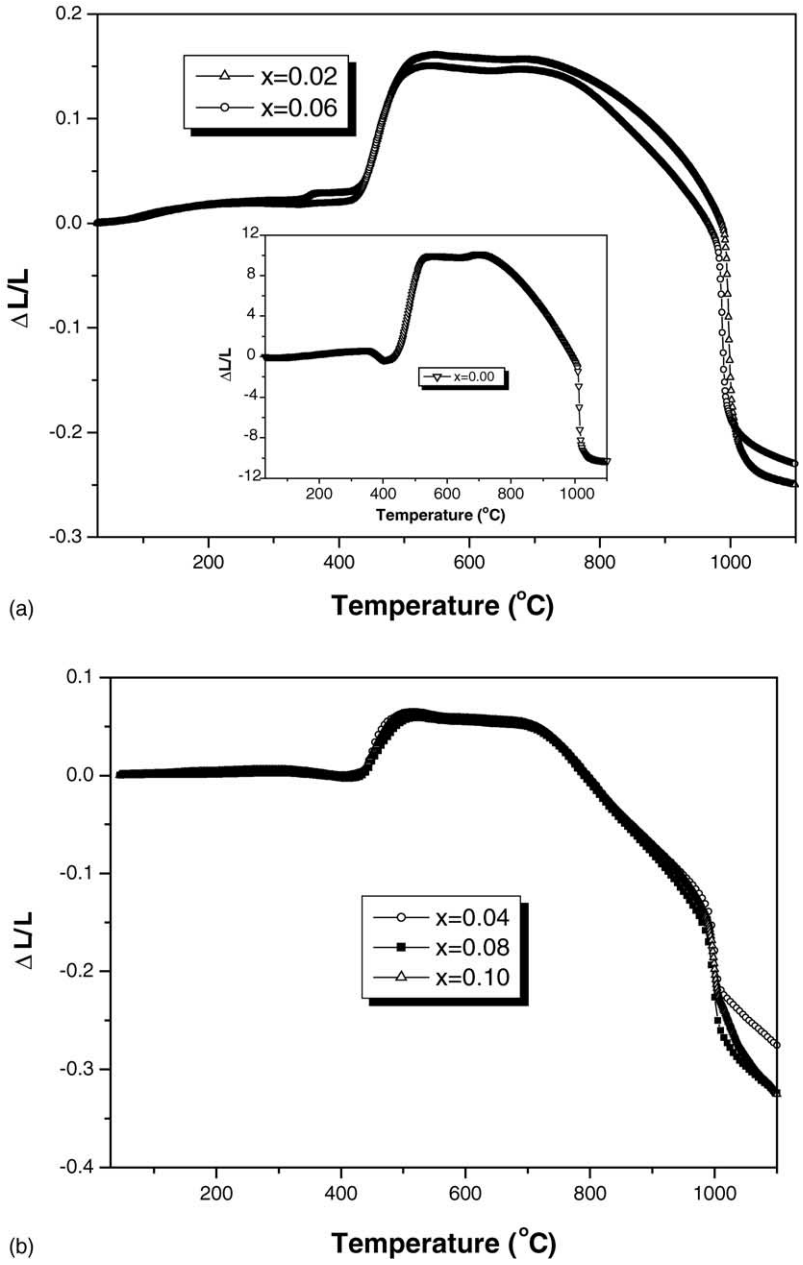

Fig. 1. Sintering shrinkage curves of samples $(La_{1-x}Ba_x)_2Mo_2O_{9-\delta}$. (a) x = 0.00, 0.02 and 0.06 and (b) x = 0.04, 0.08 and 0.10.

the $(La_{1-x}Ba_x)_2Mo_2O_{9-\delta}$ samples have reached sintering temperature. The relative density has reached to 95% of the theoretical density for the samples sintered at 950 °C for 12 h (see Table 1).

3.2. Effect of Ba doping on crystal structures of the samples

The XRD pattern of the samples $(La_{1-x}Ba_x)_2Mo_2O_{9-\delta}$ (x = 0.02–0.10) is shown in Fig. 2. It can be seen from Fig. 2 that the doped samples present $La_2Mo_2O_9$ phase, and two small, extra peaks were detected between (2 1 0) and (2 1 1) lines

Table 1
Cell parameters and density for $(La_{1-x}Ba_x)_2Mo_2O_{9-\delta}$ investigated in this study[a]

Composition	a (Å)	V_{cell} (Å^3)	ρ_{TD} (g/cm^3)	ρ_{SD} (g/cm^3)	ρ_{RD} (%)
x = 0.02	7.1622	367.40	5.546	5.158	93.0
x = 0.04	7.1573	366.65	5.554	5.172	93.1
x = 0.06	7.1804	370.21	5.497	5.217	94.9
x = 0.08	7.1855	371.00	5.482	5.220	95.2
x = 0.10	7.1818	370.42	5.487	5.234	95.4

a: cubic lattice constant; V_{cell}: cell volume; ρ_{TD}: theoretical density; ρ_{SD}: sintered density and ρ_{RD}: relative density.

[a] Estimated standard deviations for cell parameters are less than 0.0005 Å, Z = 2.

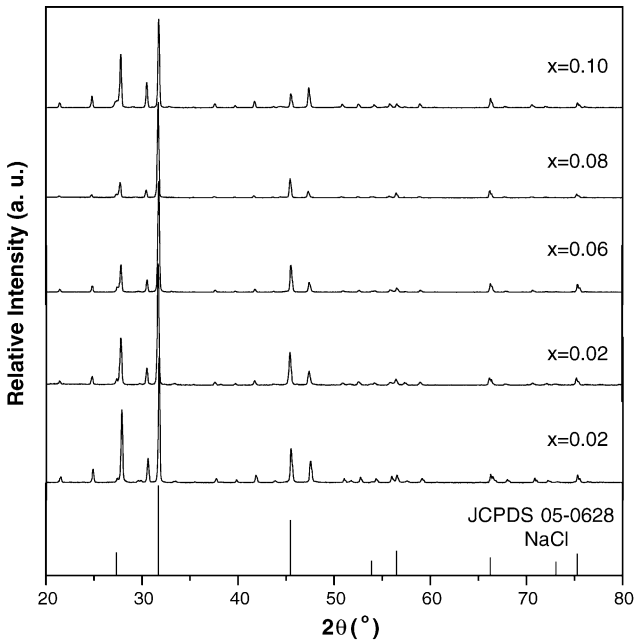

Fig. 2. XRD of samples $(La_{1-x}Ba_x)_2Mo_2O_{9-x}$($x$ = 0.02–0.10).

and (2 1 1) and (2 2 0) lines. The two small extra peaks correspond to a superstructure related to β-$La_2Mo_2O_9$, which has been observed by Goutenoire et al. [6] using neutron diffraction patterns. The small extra peak between (2 1 0) and (2 1 1) lines was also detected in fluorine-doped $La_2Mo_2O_9$ [10]. This further shows that the structures of Ba-doped $La_2Mo_2O_9$ samples are related to the high temperature form of β-$La_2Mo_2O_9$. Therefore, the cubic phase was adopted to determine the lattice constants of Ba-doped $La_2Mo_2O_9$ (see Table 1). No other extra peaks were detected in Ba-doped $La_2Mo_2O_9$ samples, although small diffraction peaks (2θ = 44.42 and 76.08, was indexed as La_2BaO_x) appeared in the XRD pattern of the sample with x = 0.10, showing that Ba in $La_2Mo_2O_9$ has a high solid solution limit [13]. Fig. 3 shows the relationship between lattice constants and Ba doping content. It can be seen that the lattice constant first decreases (x < 0.04), increases (0.04 < x < 0.08), and then decreases again (x > 0.08) with the increasing of Ba doping content. Table 1 presents the lattice constant and theoretical density of $(La_{1-x}Ba_x)_2Mo_2O_{9-\delta}$ compounds calculated using Oxford Cryosystems software. The nature of the solid solutions of Ba substituted for La site can be determined through comparison of the theoretical density and sintered density, namely, substituted solid solution. The lattice constant of $La_2Mo_2O_9$ is 7.155 Å (JCPDS#28-0509). Because the ionic radius of Ba^{2+} is larger than that of La^{3+} (nine-fold coordination, 1.47 Å for Ba^{2+} and 1.216 Å for La^{3+} [18]), the lattice constant would be expanded when Ba^{2+} is substituted for La^{3+} in oxide-ion conductor $La_2Mo_2O_9$. Therefore, the lattice constants for all Ba-doped samples are increased. It is easy to understand that the lattice constants increase with the increasing of Ba doping contents for 0.04 < x < 0.08. However, an abnormal phenomenon occurred over the range of 0.02 < x < 0.04. That is, the lattice constant was decreased as Ba doping content was increased. This may be because the relative contents of oxygen vacancy ($Vo^{\bullet\bullet}$) and localized defect associations (e.g. $\{Ba'_{La}\ Vo^{\bullet\bullet}\}$ and $\{La'_{La}\ Vo^{\bullet\bullet}\}$) have changed with the increasing of Ba doping content. That is, the defect associations began to form when the dopant content reached a certain dopant content x [19]. While the oxygen vacancy is believed to produce a larger lattice contraction than defect associations [20], therefore, the lattice constant decreased over a range of 0.02 < x < 0.04. When the Ba doping content was increased to 8%, the lattice constant presented a maximum of 7.1855 Å. When the Ba doping content was increased to 10%, the lattice constant decreased to 7.1818 Å, which was close to the result of 7.1878 Å reported by Goutenoire et al. [7]. The lattice constant decreased with the increasing of Ba doping content for x > 0.08, this means that a solid solution limit was reached for Ba in $(La_{1-x}Ba_x)_2Mo_2O_{9-\delta}$ solid solutions. These results indicate that a solid solution limit of Ba in $(La_{1-x}Ba_x)_2Mo_2O_{9-\delta}$ lies at around x = 0.08. In addition, it can be seen from the Table 1 that the presence of vacancies in the cell induces a low density for Ba-doped $La_2Mo_2O_9$. The measured density for $La_2Mo_2O_9$ sintered at 900 °C for 12 h is 5.555 g/cm^3, which is in good agreement with the result as reported by Goutenoire et al. [14].

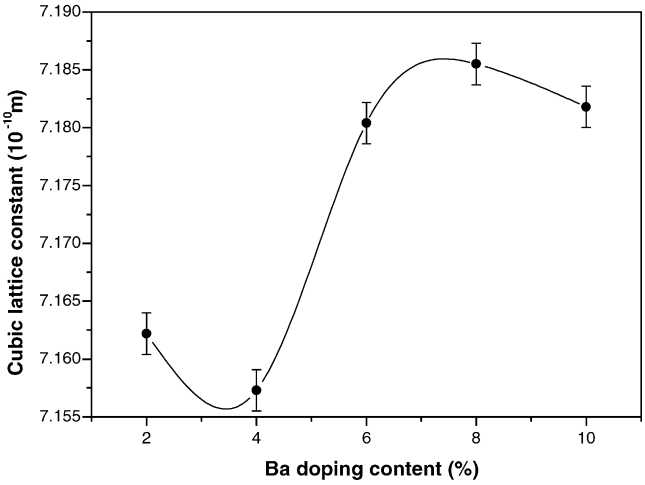

Fig. 3. Relationship between lattice constant and Ba doping content.

3.3. Effect of Ba doping on phase transition of samples

Figs. 4 and 5 show the thermal expansion (Technical Alpha) and thermal expansion coefficient (Physical Alpha) curves for the sample of $(La_{1-x}Ba_x)_2Mo_2O_{9-\delta}$ (x = 0.00–0.10). It can be seen from Fig. 4 that an obvious volume change occurs in the thermal expansion curve from 550 to 560 °C for $La_2Mo_2O_9$ sample. The phase transition temperature is 555 °C (as demonstrated by the Physical Alpha curve in Fig. 5), which corresponds to the first-order transition of the $La_2Mo_2O_9$. The phase transition temperature of the $La_2Mo_2O_9$ was about 580 °C as reported by Lacorre et al. [5] using differential thermal analysis, while Wang and Fang

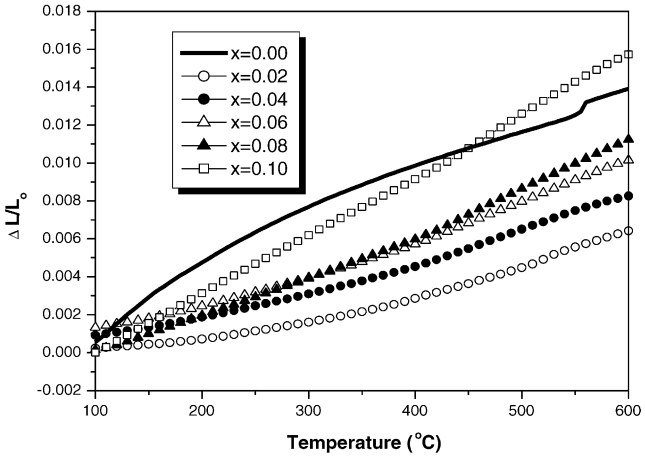

Fig. 4. Thermal expansion curves of samples $(La_{1-x}Ba_x)_2Mo_2O_{9-\delta}$ (x = 0.00–0.10).

[11,21] reported that it was at 560 °C using internal friction and differential scanning calorimetry. The difference might be due to the different experimental conditions used, such as heating rate (a heating rate of 10 °C/min was used in Lacorre et al.'s experiment, and 5 °C/min in Wang et al.'s experiment). It can be seen from Fig. 5 that, in Ba-doped samples, a slight structural phase transition can still be detected for the sample with $x = 0.02$, and the transition temperature leans toward low temperature at about 522 °C. When $x > 0.02$, no phase transition is detected for all Ba-doped samples. This means that the structural phase transition in $La_2Mo_2O_9$ can be suppressed completely as Ba doping content is more than 0.02.

3.4. Effect of Ba doping on electrical properties of samples

3.4.1. Complex impedance spectra of samples

The complex impedance spectra measured at different temperature for the sample $(La_{1-x}Ba_x)_2Mo_2O_{9-\delta}$ with x = 0.08 are shown in Fig. 6. Similar complex impedance spectra for all other samples corresponding to the four compositions studied were obtained as shown in Fig. 6. An equivalent circuit, which comprised of resistances and constant phase elements (CPE) in parallel and series as reported [10], was adopted. It can be seen from Fig. 6, that when temperature is below 450 °C, two broadened semicircles appear in the complex plane. The associated capacitance values of the left semicircles are 8.1×10^{-12}, 6.4×10^{-12}, 4.9×10^{-12} and 1.4×10^{-12} F/cm, respectively, which is a typical of a grain component. The ones of the right semicircles are 1.0×10^{-7}, 1.4×10^{-7}, $1.8 \times 10^{-7}$and 4.6×10^{-7} F/cm, respectively, which is typical of an electrolyte-electrode interface component [22]. There was no evidence of a grain boundary semicircle that might be attributable to grain boundary impedances. It is thus clear that compared to the grain resistance, the grain boundary resistance is much smaller, and as the temperature increased, the grain resistance gradually decreased. When the temperature is over 600 °C, there is only one arc with a tail of corresponding interface impedance, which is due to ion and electron transference at the interface between electrolyte and electrodes, left in the impedance spectra. The associated capacitance values of the arcs above the real axes are 3.0×10^{-5}, 2.9×10^{-5}, 3.0×10^{-5}, 3.8×10^{-5}, 5.2×10^{-5} and 6.1×10^{-5} F/cm, respectively, which are characteristic of ionic polarization phenomena at the blocking electrodes [23]. These results support the fact that the conducting species in the Ba-doped $La_2Mo_2O_9$ material is predominately ionic.

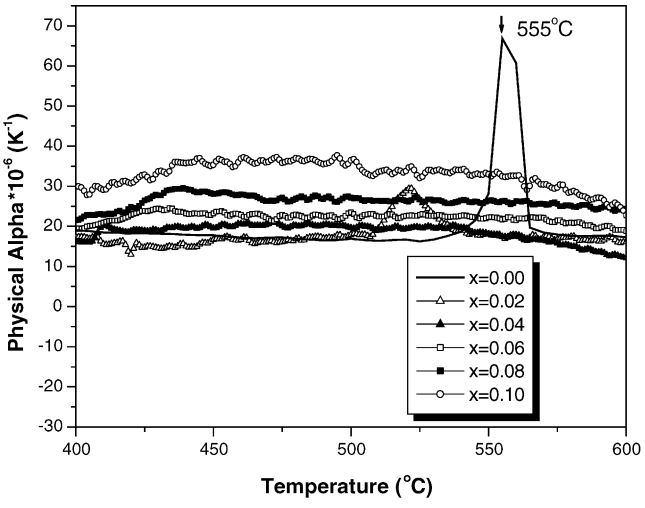

Fig. 5. Thermal expansion coefficient curves of samples $(La_{1-x}Ba_x)_2Mo_2O_{9-\delta}$ (x = 0.00–0.10).

3.4.2. Arrhenius plots of samples

Fig. 7 shows Arrhenius plots of conductivity for the $(La_{1-x}Ba_x)_2Mo_2O_{9-\delta}$ (x = 0.00–0.10) samples. It can be seen from the inset in Fig. 7 that the Arrhenius plot of conductivity for the $La_2Mo_2O_9$ sample has an abrupt change over the range of 500–600 °C, i.e. a broken line is present on this curve, which corresponds to a structural phase transition from α-$La_2Mo_2O_9$ to β-$La_2Mo_2O_9$ [6]. Other curves for Ba-doped samples have become very smooth over the same temperature range. This indicates that doping Ba for La in $La_2Mo_2O_9$ has suppressed the structural phase transition.

3.4.3. Conductivity of samples

Table 2 is the conductivity of $(La_{1-x}Ba_x)_2Mo_2O_{9-\delta}$ samples measured at different temperatures. It can be seen that the conductivity of the samples first decreases, then increases, and decreases again, with the increasing of Ba doping content. This is in agreement with the relationship between the lattice constant and the dopant content. That is,

Table 2
Conductivity of samples $(La_{1-x}Ba_x)_2Mo_2O_{9-\delta}$ at different temperatures

Measured temperature (°C)	Conductivity of samples (S/cm)				
	x = 0.02	x = 0.04	x = 0.06	x = 0.08	x = 0.10
800	0.050	0.029	0.046	0.046	0.022
850	0.059	0.036	0.059	0.075	0.025

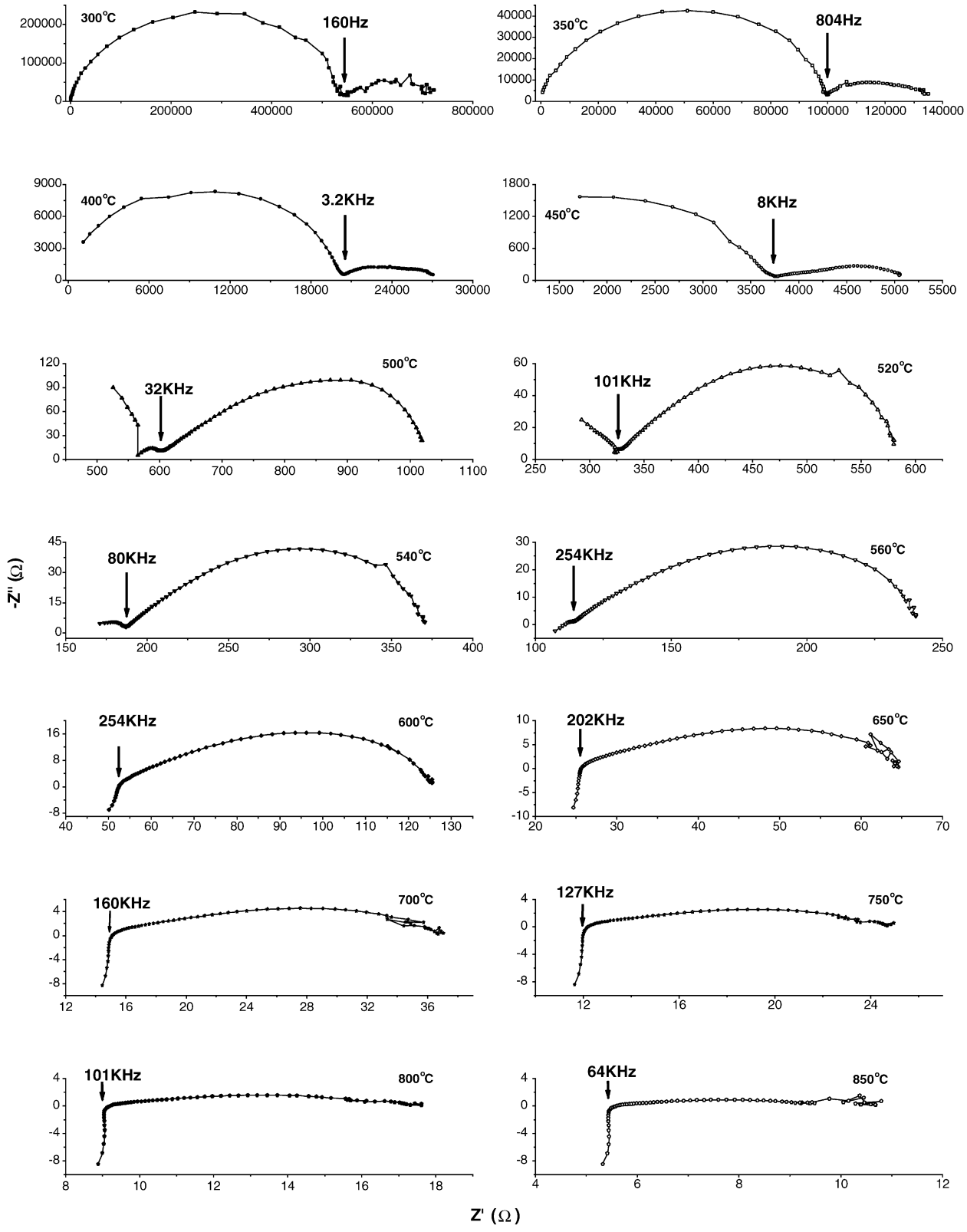

Fig. 6. Complex impedance spectra of sample $(La_{1-x}Ba_x)_2Mo_2O_{9-\delta}$ ($x = 0.08$).

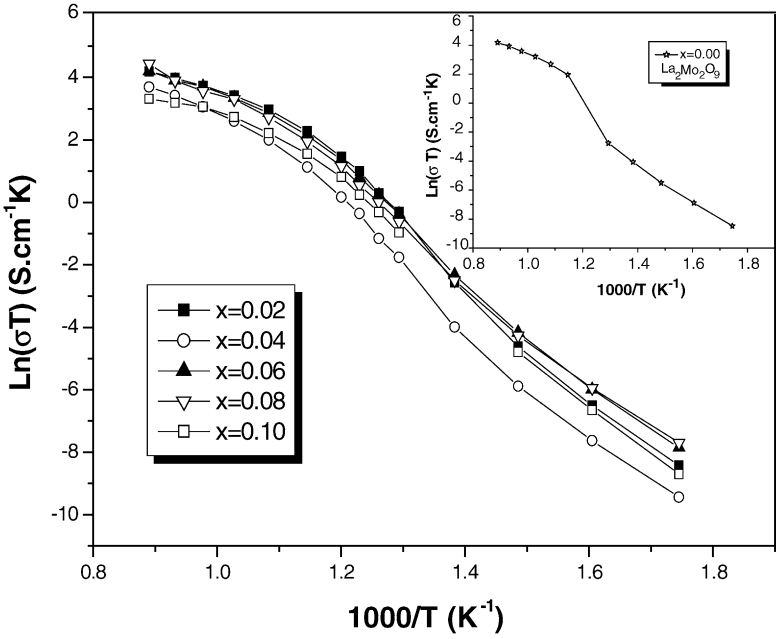

Fig. 7. Arrhenius plots of conductivity for samples $(La_{1-x}Ba_x)_2Mo_2O_{9-\delta}$ (x = 0.00–0.10).

with the increasing of unit cell volume, the conductivity increases. This is because the larger the unit cell volume is, the easier the oxygen ions diffuse, and the conductivity will thus increase. This further confirms that the solid solution limit of Ba in $(La_{1-x}Ba_x)_2Mo_2O_{9-\delta}$ lies at around x = 0.08. In the series of Ba-doped samples, the conductivity of the samples exhibits a maximum at x = 0.08, with the conductivities of 0.046 and 0.075 S/cm at 800 and 850 °C, respectively, which is higher than that of yttria-stabilized zirconia at the same temperature [24]. In this study, the conductivity of the Ba-doped $La_2Mo_2O_9$ is also higher than that of $(La_{2-x}Ba_x)Mo_2O_{9-\delta}$ with x = 0.10 reported by Goutenoire et al., which has a conductivity of 2.74×10^{-3} S/cm at 800 °C [7]. This is mainly because the oxygen vacancy substituted by Ba in $(La_{1-x}Ba_x)_2Mo_2O_{9-\delta}$ is more than that in $(La_{2-x}Ba_x)Mo_2O_{9-\delta}$ at the same value of x. Thus, the appropriate Ba doping not only can suppress the structural phase transition in $La_2Mo_2O_9$, but also can improve the electrical property. It provides the possibility of extending the applications of $La_2Mo_2O_9$ oxide-ion conductor.

4. Conclusions

The oxide-ion conductors $(La_{1-x}Ba_x)_2Mo_2O_{9-\delta}$ (x = 0.02–0.10) were prepared by solid-state reaction method. The sintering investigation shows that the forming process of $La_2Mo_2O_9$ phase in samples presents an expansion process due to the introduction of oxygen vacancy. X-ray diffraction results show that Ba in $La_2Mo_2O_9$ has a high solid solution limit. The lattice constant first decreases, then increases, and decreases again with the increasing of Ba doping content. When Ba doping content is 8%, the lattice constant presents a maximum of 7.1855 Å. This indicates that the solid solution limit of Ba in $(La_{1-x}Ba_x)_2Mo_2O_{9-\delta}$ lies at around x = 0.08. When x > 0.02, both electrical and thermal results have demonstrated that the structural phase transition in $La_2Mo_2O_9$ oxide-ion conductor can be completely suppressed through the substitution of Ba for La site, which stabilizes the high temperature phase to room temperature. As the dopant content reaches x = 0.08, the sample of $(La_{1-x}Ba_x)_2Mo_2O_{9-\delta}$ exhibits an optimal electrical property, and the conductivity of the sample was 0.046 and 0.075 S/cm at 800 and 850 °C, respectively. The structural phase transition can be effectively suppressed through appropriately substituting Ba^{2+} for La^{3+}.

Acknowledgements

This work was supported by Jilin Province Department of Science and Technology. The authors gratefully appreciate the reviewer's valuable comments and suggestions on our manuscript.

References

[1] N.Q. Minh, J. Am. Ceram. Soc. 76 (1993) 563.
[2] T. Ishihara, H. Matsuda, Y. Takita, J. Am. Chem. Soc. 116 (1994) 3801.
[3] F. Abraham, J.C. Boivin, G. Mairesse, G. Nowogrocki, Solid State Ionics 41–44 (1990) 934.
[4] H.L. Tuller, Solid State Ionics 94 (1997) 63.
[5] P. Lacorre, F. Goutenoire, O. Bohnke, R. Retoux, Y. Laligant, Nature 404 (2000) 856.

[6] F. Goutenoire, O. Isnard, R. Retoux, P. Lacorre, Chem. Mater. 12 (2000) 2575.
[7] F. Goutenoire, O. Isnard, E. Suard, O. Bohnke, Y. Laligant, R. Retoux, P. Lacorre, J. Mater. Chem. 11 (2001) 119.
[8] P. Lacorre, Solid State Sci. 2 (2000) 755.
[9] S. Georges, F. Goutenoire, Y. Laligant, P. Lacorre, J. Mater. Chem. 13 (2001) 2317.
[10] A. Arulraj, F. Goutenoire, M. Tabellout, O. Bohnke, P. Lacorre, Chem. Mater. 14 (2002) 2492.
[11] X.P. Wang, Q.F. Fang, Solid State Ionics 146 (2002) 185.
[12] Q.F. Fang, X.P. Wang, G.G. Zhang, Z.G. Yi, J. Alloy Comp. 355 (2003) 177.
[13] R. Subasri, D. Matusch, H. Näfe, F. Aldinger, J. Euro. Ceram. Soc. 24 (2004) 129.
[14] S. Georges, F. Goutenoire, F. Altorfer, D. Sheptyakov, F. Fauth, E. Suard, P. Lacorre, Solid State Ionics 161 (2003) 231.
[15] Q.B. Bo, J. Feng, H.Y. Wang, J. Meng, Chin. Chem. Lett. 14 (2003) 197.
[16] P.H. Larsen, P.V. Hendriksen, M. Mogensen, J. Thermal Anal. 49 (1997) 1263.
[17] Y.L. Huang, T.M. He, Y. Ji, J.X. Wang, D.Y. Wang, J. Rare Earths 22 (2004) 113 (in Chinese).
[18] R.D. Shannon, Acta Cryst. A 32 (1976) 751.
[19] W. Huang, P. Shuk, M. Greenblatt, Chem. Mater. 9 (1997) 2240.
[20] L.P. Li, G.S. Li, Y.L. Che, W.H. Su, Chem. Mater. 12 (2000) 2567.
[21] X.P. Wang, Q.F. Fang, J. Phys. Condens. Mater. 13 (2001) 1641.
[22] J.G. Fletcher, A.R. West, J.T.S. Irvine, J. Electrochem. Soc. 142 (1995) 2650.
[23] C.K. Lee, C.S. Ong, Solid State Ionics 117 (1999) 301.
[24] L. Cong, T. He, Y. Ji, P. Guan, Y. Huang, W. Su, J. Alloy Comp. 348 (2003) 325.